

3D Surface Estimation and Model Construction From Specular Motion in Image Sequences

Jiang Yu Zheng, Yoshihiro Fukagawa, and Norihiro Abe

Abstract—This work reconstructs a 3D graphics model of an object with specular surfaces by its rotation. Continuous images are taken to measure highlights on the smooth surfaces and their motion. Coplanar extended lights determine a *plane of rays* to produce a highlight stripe on the object. 3D surfaces are then recovered from the moving stripe. We investigate global motion characteristics of the highlights in the *Epipolar-plane images* so as to qualitatively identify surface types and control the modeling process. Under single and multiple plane-of-rays illuminations, we give two quantitative approaches for surface and normal recovery which use highlight orientation in the image and highlight motion in the Epipolar-Plane images. The computations employ a first-order differential equation and linear equations, respectively.

Index Terms—Specular motion, highlight, shape estimation, model recovery, epipolar-plane images, qualitative shape identification.

1 INTRODUCTION

CURRENT techniques of 3D shape measurement using computer vision mainly deal with diffused surfaces. Even laser range finders cannot determine the correct shape of a surface with strong specular reflectance [12]. In the real world, however, there are plenty of objects from industrial parts to daily goods containing specular reflectance. The objective of our work is to estimate 3D shapes and construct graphics models of such objects. The results will be used in CAD, virtual reality, and multimedia applications.

It is well known that a specularly reflected pattern will shift on a smooth surface either when the viewpoint or the object moves. The image motion differs from that of surface textures. This is used as a cue by humans in perceiving specularity. In the case where little texture appears on the surface, specularly reflected patterns and highlights play an important role in the perception of the surface shape of an object. We deal with smooth surfaces on which a highlight is observable under illumination. The materials which satisfy such a condition can be smooth metal, opaque glass, ceramic, or plastic.

Contributions on specularity so far, include separation of Lambertian and specular reflecting components [3], computation of surface normals [1] by photometric methods, analysis of disparity and motion of specularly reflected points from several images which constrain surface shape [4], [5], and computing up to a 3D curve on a simple surface by moving the camera [6], [11]. The objective of this work is to first reconstruct the surface and then a 3D model of an object [8], [10]. This is a most significant step to bridging computer vision to real applications.

In order to obtain a 3D model, we rotate the object so as to observe all surfaces. Rotation is the simplest mechanism to realize. To

simplify the problem, we use orthogonal projection so that the positions of visible features are not related to viewing distance of the camera, which is intrinsic in dealing with specular motion. In order to determine a surface and then an object model, we use extended lights that project highlight stripes on the object. The stripe gradually shifts across the surfaces during the rotation and passes most points once. By following the highlight in the images, the shape of the underlying surface is recovered. The lights are set in a plane containing the rotation axis. We call the plane the *plane of rays*.

The specular motion is captured in *Epipolar-Plane Images* (EPI) projected from rotation planes at different heights. In this paper, we focus on two kinds of visual features—fixed features from corners and textures, and specularly reflected features including highlights. A projected highlight in the EPI moves over trajectories of surface points on the same rotation plane. We compute the positions of the surface points from the tracked highlight trace. The object model is then obtained by combining the shapes at all the rotation planes. The advantages of using EPIs rather than using only original images are

- 1) the easy tracking of highlights which split, merge, and change size in the image sequence,
- 2) uniformed processing performed on each rotation plane, and
- 3) spatial tracing of temporal highlight motion which indicates the curvature signs of surfaces.

This paper gives both qualitative and quantitative results of shape recovery from the motion of specularly reflected points. Qualitatively, we identify shapes on a rotational plane as corner, convex, planner, and concave types. This is done by comparing image motions between a highlight and the surface points it crosses. The points where curvature changes sign can also be located directly. Second, we find that under multiple planes of rays, the density of highlight traces in an EPI is related to shape curvature in the rotation plane. The greater the curvature, the denser the traces of the highlights viewed become.

Quantitatively, we extract direction of a highlight stripe in the image and highlight motion in the rotation planes. They provide 3D shape information in spatial and temporal ways. Two shape recovery methods are given.

- 1) Under two planes of rays, two traces of highlights may be visible in the EPIs. Linear equations can yield 3D positions of moving highlights on the surface.
- 2) Under one plane of rays, a first-order differential equation which can describe highlight motion in the EPI. The computation of object shape starts from any known fixed point or contour which can provide the initial condition to the solution of the differential equation.

2 BASIC ASSUMPTIONS AND CONSTRAINTS

2.1 Geometry of Camera and Object

An object rotates around an axis \mathbf{R} and the camera viewing direction \mathbf{v} is aligned perpendicular to \mathbf{R} (Fig. 1). Continuous images are taken under orthogonal projection and a *spatial-temporal volume* is piled. We locate an object coordinate system O-XYZ so that its Y axis is on the rotation axis. Through simple calibration, the camera-centered coordinate system C-xyz can be determined so that its z axis passes through axis \mathbf{R} and its y axis is parallel to \mathbf{R} . The object starts rotating when the Z and z axes are collinear. Rotation is clockwise and the rotation angle θ of the object is known. The system C-xyz then rotates counterclockwise relative to the system O-XYZ. A surface point $\mathbf{P}(X, Y, Z)$ in the system O-XYZ is projected to $p(x, y)$ in the image frame, where the y and Y coordinates are the same. It is mapped to point $(x(\theta), y(\theta), \theta)$ in the *spatial-temporal volume* [2].

- J.Y. Zheng and N. Abe are with the Faculty of Computer Science and Systems Engineering, Kyushu Institute of Technology, 680-4 Kawazu, Iizuka, Fukuoka 820, Japan. E-mail: {zheng, abe}@mse.kyutech.ac.jp.
- Y. Fukagawa was master student at the Kyushu Institute of Technology and is currently with the Torey Corporation.

Manuscript received June 9, 1995; revised Jan. 27, 1997. Recommended for acceptance by S.K. Nayar.

For information on obtaining reprints of this article, please send e-mail to: transpami@computer.org, and reference IEEECS Log Number 104070.

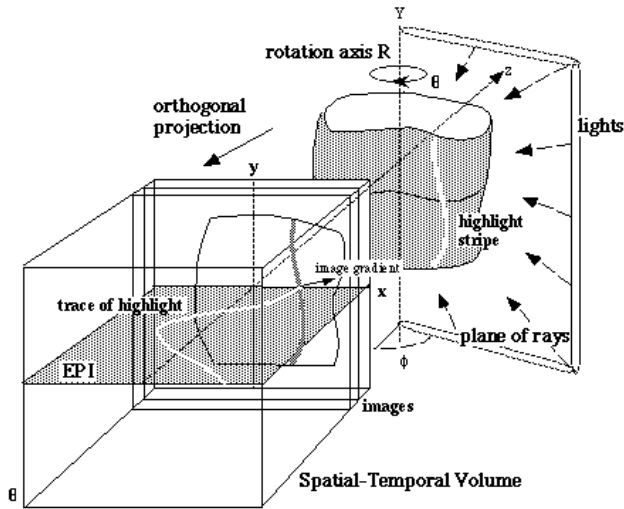


Fig. 1. Image formation geometry for shape recovery. Object is rotated and illuminated by a plane of rays. Camera direction is perpendicular.

As the object rotates, a surface point is maintained in a rotation plane. The plane is projected onto a line in the image frame continuously, from which an EPI is collected as θ increases [7]. The surface point has a moving trajectory as a sinusoidal curve (half visible in one period) in the EPI, even though it is not distinct enough to be located. One example of EPI is shown in Fig. 2, in which the motion of an object with both concave and convex surfaces is shown. According to the camera geometry (Fig. 3), the camera axis is $\mathbf{z} = (-\sin \theta, \cos \theta)$ in the sub-system O-XZ. The image position of a point P visible at rotation angle θ is

$$\mathbf{x}(\theta) = \mathbf{P} \cdot \mathbf{x} = X(\theta) \cos \theta + Z(\theta) \sin \theta \quad (1)$$

which is a sinusoidal function of θ over a period of 2π . The \mathbf{x} here is a unit vector of the x axis in the system C-xyz.

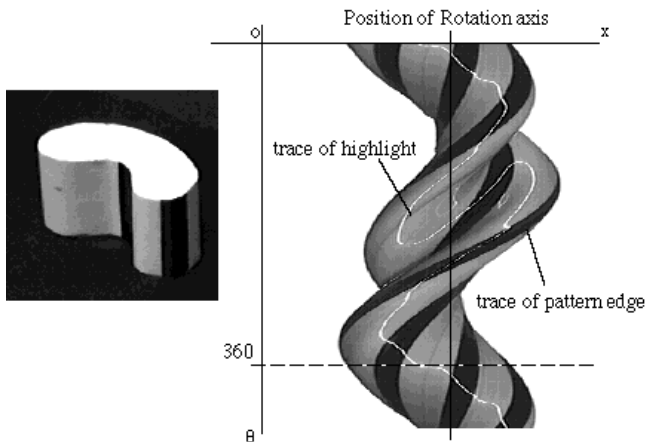


Fig. 2. One example of EPI from a rotating plastic object. Dark stripes are traces of black patterns on the surface. A highlight trace crosses all traces of surface points on the rotation plane.

2.2 Plane-of-Rays Illumination and Normal Estimation

Extended lights are connected around the object in a half plane passing axis R (Fig. 1). The lights are far away from the object compared with the object size so that the rays from a light point to all surface points have the same direction. The rays centralized at

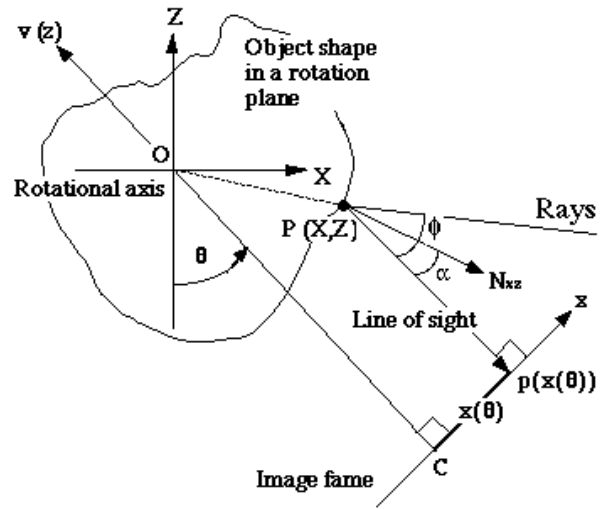


Fig. 3. One cross section of an object in a rotation plane.

the object are, hence, coplanar. We call the half plane the *plane of rays* (POR). It can also be realized by one linear light parallel to the rotation axis if its length is long. Rather than a point feature or a point light [4], [5], [6], [11], extended lights can highlight a surface stripe whose points have different normals.

We will compute the surface normal at a highlight point. Denoting the azimuth angle of the plane of rays from direction \mathbf{V} ($= -\mathbf{v}$, inverse of camera direction) by ϕ (counterclockwise), Fig. 4 depicts a Gaussian sphere located at axis R for analysis. Denoting the normal at a highlight point as $\mathbf{N}(\cos \beta \sin \alpha, \sin \beta, -\cos \beta \cos \alpha)$ in the camera system C-xyz, where α and β are the azimuth angle from \mathbf{V} and the angle of \mathbf{N} from the rotation plane, respectively, and by denoting the corresponding ray as $\mathbf{L}(\cos \phi \sin \phi, \sin \phi, -\cos \phi \cos \phi)$, we have the relation $\angle \mathbf{VCN} = \angle \mathbf{NCL}$ because the angle of incidence is equal to the angle of reflection in specular reflection. By changing ϕ in $(-\pi/2, \pi/2)$ to generate different rays, the normals of highlighted points compose a curve on the sphere. We will see the azimuth angle α is uniquely determined from angle β as follows. According to the constraint $\angle \mathbf{VCN} = \angle \mathbf{NCL}$ and the constraint that \mathbf{V} , \mathbf{N} , and \mathbf{L} are coplanar, we have

$$\mathbf{V} \times \mathbf{N} = \mathbf{N} \times \mathbf{L} \quad (2)$$

which can be written in detail as

$$\begin{aligned} & [0, 0, -1] \times [\cos \beta \sin \alpha, \sin \beta, -\cos \beta \cos \alpha] \\ &= [\cos \beta \sin \alpha, \sin \beta, -\cos \beta \cos \alpha] \times [\cos \phi \sin \phi, \sin \phi, -\cos \phi \cos \phi] \end{aligned} \quad (3)$$

Eliminating ϕ in the subequations of (3), we deduce the relation between α and β as

$$\sin^2 \alpha + \sin^2 \phi \tan^2 \beta = \sin^2(\phi - \alpha) \quad (4)$$

If the plane of rays is parallel with the camera direction ($\phi = 0$ in (4)), angle β can be any value in the range $[-\pi/4, \pi/4]$ and α is 0. We can also intuitively conclude from Fig. 4 that every surface point whose zenith angle of normal is within $[-\pi/4, \pi/4]$ will be highlighted, as long as it rotates in the camera direction. If, on the other hand, $\phi \neq 0$, highlighted angle β will be in the range $[-\pi/4, \pi/4]$, which can be represented in terms of α by

such points along a highlight trace (e.g., A, B, C, D in Fig. 5c2), we can segment the shapes which have different curvature signs. On a convex shape, the highlight stays on the side of light during the rotation. It moves slower than the surface points and its trace crosses with those of the surface points (e.g., C, F, D in Fig. 5c3). On a concave shape, however, the highlight moves with a higher image velocity in the same direction as the surface points (e.g. E, G in Fig. 5c2). We can identify which type of shape a highlight trace is moving on by checking how it crosses with a trace of a fixed point. As the absolute value of curvature becomes high, the shape becomes closer to being a corner. The highlight trace is then close to a sinusoidal corner trace (C, D in Fig. 5c3) and disappears at an ideal corner ($c = \pm\infty$). A corner trace, hence, connects highlight traces in the EPI.

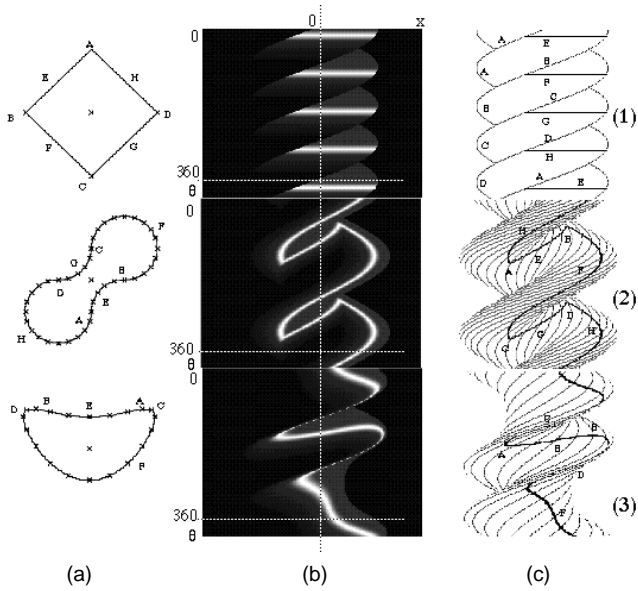


Fig. 5. Simulated traces of surface points and highlights when cylinders rotate clockwise. (a) Three shapes containing corner, plane, convex and concave shapes (* sign: surface points, × sign: rotation axis) and the motion of specular points. The camera axis is aligned with the Z axis when objects start rotation. (b) EPIs generated from the three shapes by Phone's model. Both specular reflectance and diffused reflectance exist. The light direction ϕ is at 60 degrees to the right of the camera. (c) Traces of surface points (narrow curves) and highlight traces (bold curves) labeled to be consistent with the shapes on which they are moving.

The proof of above statements is given next. By using the relation of X'_θ and Z'_θ in (9) and computing Z''_θ in terms of X , we obtain the curvature of a shape in the rotation plane as

$$\begin{aligned}
 c(\theta) &= \left(X'_\theta Z''_\theta - Z'_\theta X''_\theta \right) \left(X'^2_\theta Z'^2_\theta \right)^{-3/2} = \\
 &= \left(X'^2_\theta + \tan^2(\theta + \alpha) X''^2_\theta \right)^{-3/2} \\
 &\times \left(X'_\theta \left(X''_\theta \tan(\theta + \alpha) + X'_\theta \sec^2(\theta + \alpha) (\partial\alpha/\partial\theta + 1) \right) \right. \\
 &\quad \left. - X''_\theta \tan(\theta + \alpha) X''_\theta \right) \\
 &= \frac{\cos(\theta + \alpha)}{X'_\theta} \left(\frac{\partial\alpha(\theta)}{\partial\theta} + 1 \right) \quad (10)
 \end{aligned}$$

The image velocity of a surface point under the highlight has a negative value since the object rotates clockwise. Using (1) and (9), the difference $v_h - v$ is computed as

$$\begin{aligned}
 v_h(\theta) - v(\theta) &= \frac{\partial X_h(\theta)}{\partial\theta} - \frac{\partial X(\theta)}{\partial\theta} \\
 &= \frac{\partial}{\partial\theta} (X(\theta) \cos\theta + Z(\theta) \sin\theta) - \frac{\partial}{\partial\theta} (X \cos\theta + Z \sin\theta) \\
 &= \frac{\partial X(\theta)}{\partial\theta} \cos\theta + \frac{\partial Z(\theta)}{\partial\theta} \sin\theta = \frac{X'_\theta(\theta) \cos\alpha}{\cos(\alpha + \theta)} = \frac{\cos\alpha}{c(\theta)} \left(\frac{\partial\alpha}{\partial\theta} + 1 \right) \quad (11)
 \end{aligned}$$

which is related to the curvature. Letting $c(\theta)$ equal the various values described above, (11) gives the relation of highlight motion with respect to the surface points.

3.3 Global Highlight Motion with Splitting and Merging

Analyzing global appearance of highlight traces is important in model construction. We recognize the combination of different surfaces from the connections of traces in the EPI [10]. During the rotation, highlights split and merge, appear and disappear at zero curvature points, and move along convex and concave surfaces. Fig. 6 depicts the cross-sections of two shapes with convex-concave-convex and corner-linear-convex combinations. On the first shape, highlight A moves on the first convex surface. Meanwhile, point B with zero curvature is highlighted and then splits into two highlights C and D moving on the concave and the second convex shapes separately. Point D then merges with A at another zero curvature point E and disappears. This splitting and merging process can be observed from traces of highlights in the corresponding EPI (Fig. 6a2). Similarly, we can qualitatively determine the highlight trace from the corner-linear-convex combination (Fig. 6b). It is sinusoidal curve A followed by horizontal segment AB, and then a trace on a convex shape.

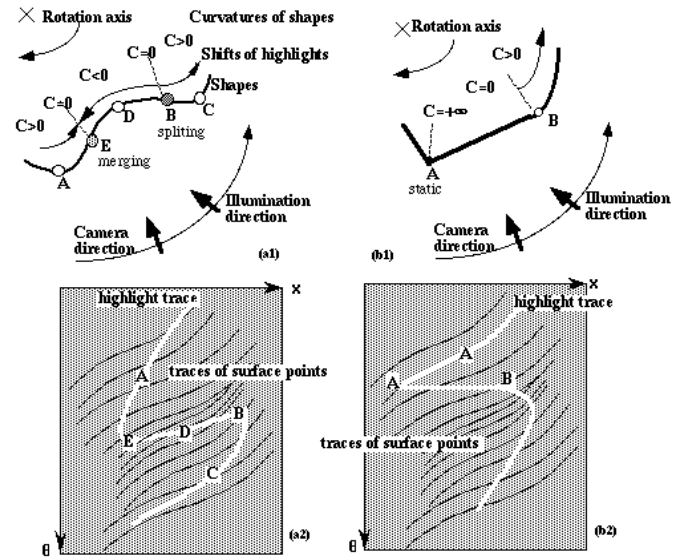


Fig. 6. Connection of highlight traces according to the combination of shapes. (a) Convex-concave-convex shape, (b) Corner-plane-convex shape. (1) Highlight movement on the surfaces, (2) Highlight traces in EPIs.

As a result, a highlight shifts on object surfaces and passes all surface points at least once if no occlusion of the ray occurs. With either fixed or shifting points on the object surfaces, a queue of highlight traces in EPI crosses the traces of all surface points in one period of rotation. We, hence, attempt to compute positions of surface points from this queue.

3.4 Motion Characteristics of Multiple Highlights

If multiple planes of rays are set around, multiple reflected highlights are visible. For the two planes of rays at ϕ_1 and ϕ_2 where

$\phi_1 > \phi_2$, a point will, in turn, reflect them when its normal rotates to angle α_1 and then to angle α_2 in the system C-xz; having a delay $\Delta\alpha = \alpha_1 - \alpha_2 > 0$. Because of the delay, the two traces of the highlights will never cross each other in the EPI. At either concave or convex corner, these traces merge into a corner trace. Fig. 7 shows a simulation that displays the traces of multiple highlights.

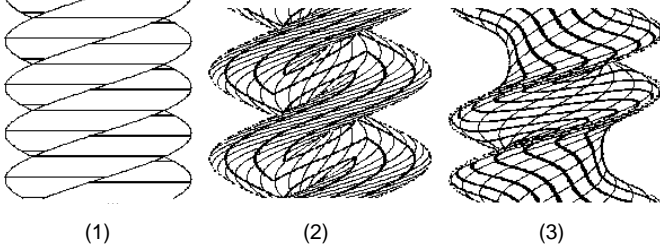


Fig. 7. Traces of multiple highlights over traces of surface points. The shapes generating (1) (2) and (3) are the same as those in Fig. 5. The intervals between planes of rays are 40 degrees for (1) and (2), 30 degrees for (3), respectively. Highlight traces are delayed one by one along the traces of the surface points.

Although multiple traces of highlights will not cross each other, we will see that their density depends on the curvature of the shape in the rotation plane. Highlight traces become close to each other on the surface when the absolute value of curvature tends to be great. Given two planes of rays separated by angle $\Delta\phi$, the distance between the two highlights is Δx . The density at angle θ is defined as the inverse of the distance when $\Delta\phi$ approaches to zero, which is

$$\text{density}(\theta) = \lim_{\Delta\phi \rightarrow 0} |\Delta x / \Delta\phi|^{-1} = |\partial x / \partial\phi|^{-1} = \left[X'_\phi \cos\theta + Z'_\phi \sin\theta \right]^{-1} \quad (12)$$

It is only influenced by shape and not by the interval between two PORs. On the other hand, the curvature is computed in terms of ϕ as

$$\begin{aligned} c(\phi) &= \left(X'_\phi Z''_\phi - Z'_\phi X''_\phi \right) \left(X'^2_\phi + Z'^2_\phi \right)^{-3/2} = \left(X'^2_\phi + \tan^2(\theta + \alpha) X'^2_\phi \right)^{-3/2} \\ &\times \left(X'_\phi \left(X''_\phi \tan(\theta + \alpha) + X'_\phi \sec^2(\theta + \alpha) \partial\alpha / \partial\phi \right) - X'_\phi \tan(\theta + \alpha) X''_\phi \right) \\ &= \frac{\cos(\theta + \alpha)}{X'_\phi} \frac{\partial\alpha}{\partial\phi} \end{aligned} \quad (13)$$

Because (X'_ϕ, Z'_ϕ) is the motion of a highlight on the surface due to a small shift in light angle ϕ , it is along the surface tangent in the rotation plane. Its direction is then the same as the one in (9), which is from a small change in θ . The tangent direction hence is obtained as $Z'_\phi / X'_\phi = Z''_\phi / X''_\phi = \tan(\theta + \alpha)$. Using (12), (13), and the relations $c(\theta) = c(\phi)$ at the highlight point, we obtain

$$\begin{aligned} \text{density}(\theta) &= \left| X'_\phi \left(\cos\theta + Z'_\phi / X'_\phi \sin\theta \right) \right|^{-1} = \\ \frac{|\cos(\theta + \alpha)|}{X'_\phi(\phi) \cos\alpha} &= \frac{|c(\phi)|}{\partial\alpha / \partial\phi \cos\alpha} = \frac{|c(\theta)|}{(\partial\alpha / \partial\phi) \cos\alpha} \end{aligned} \quad (14)$$

which is proportional to the curvature in the rotation plane.

4 SHAPE RECOVERY WITH MULTIPLE PLANES OF RAYS

4.1 Linear Equations for Local Shape Recovery

The position of a surface point can be determined from its sinusoi-

dal trace in the EPI. For most surface points other than fixed points, however, their moving traces cannot be extracted. To determine the sinusoidal function, we need at least two highlight points on each trace of a surface point (Fig. 7). Setting two planes of rays at ϕ_1 and ϕ_2 , a surface point (X, Z) will reflect them when its normal rotates to α_1 and α_2 in the camera system C-xz. According to (1), the first highlight has its image position as

$$x_1(\theta) = X(\theta) \cos\theta + Z(\theta) \sin\theta \quad (15)$$

After the duration $\Delta\alpha = \alpha_1 - \alpha_2$, the same point reflects the second light, which gives the image position

$$x_2(\theta + \Delta\alpha) = X(\theta) \cos(\theta + \Delta\alpha) + Z(\theta) \sin(\theta + \Delta\alpha) \quad (16)$$

From (15) and (16), surface point (X, Z) can be directly computed by

$$\begin{pmatrix} X(\theta) \\ Z(\theta) \end{pmatrix} = \frac{1}{\sin\Delta\alpha} \begin{pmatrix} \sin(\theta + \Delta\alpha) & -\sin\theta \\ -\cos(\theta + \Delta\alpha) & \cos\theta \end{pmatrix} \begin{pmatrix} x_1(\theta) \\ x_2(\theta + \Delta\alpha) \end{pmatrix} \quad (17)$$

which is a very simple computation. The geometry explanation of (17) is as follows. Being constrained by two planes of rays, two lines of sight that view a specular surface point from two angles cross each other at the point, which determines the point position. In order to compute (17) for the surface shape, we compute α_1 from the image gradient at the first highlight using (8). Next, because angle β is constant for the point during the rotation, we have

$$\left(\sin^2(\phi_1 - \alpha_1) - \sin^2\alpha_1 \right) \sin^2\phi_2 = \left(\sin^2(\phi_2 - \alpha_2) - \sin^2\alpha_2 \right) \sin^2\phi_1 \quad (18)$$

from (4). It further yields

$$\Delta\alpha = \frac{1}{2} \left(2\alpha_1 - \phi_2 + \sin^{-1} \left(\frac{\sin(\phi_1 - 2\alpha_1) \sin\phi_2}{\sin\phi_1} \right) \right) \quad (19)$$

for the computation of (17). Globally, we track one highlight trace in the EPI. For each highlight point $x_1(\theta)$ on the trace, we find a point on the second highlight trace which is delayed $\Delta\alpha$ in its rotation angle. The located point $x_2(\theta + \Delta\alpha)$ is consequently the correspondence projected from the same surface point.

For a plane, its shape in the rotation plane is a line. Two horizontal traces will appear in the EPI. Because the whole plane is shiny when the normal rotates to α_1 and α_2 , the image gradient is unable to be extracted at the region. Moreover, for any highlight point on the first trace, all points on the second trace become candidates for matching. Nevertheless, we can obtain the delay $\Delta\alpha$ from the distance between the two horizontal traces in the EPI. Then we can compute α_1 from $\Delta\alpha$ using (19) and β from α_1 using (5). From either the connected non-planar shape or a possible fixed point, we can obtain a known point (X_1, Z_1) on the line whose image position is $x_1(\theta)$. According to (1) and (9), any other point (X, Z) on the line can be calculated from its image position x and $x_1(\theta)$ as

$$\begin{pmatrix} X \\ Z \end{pmatrix} = \begin{pmatrix} \cos(\theta + \alpha_1) \\ \sin(\theta + \alpha_1) \end{pmatrix} (x - x_1) + \begin{pmatrix} X_1 \\ Z_1 \end{pmatrix} \quad (20)$$

4.2 Lights Calibration and Interreflection

The azimuth angle of a POR can be obtained either from the system setting or through calibration. To locate directions ϕ_1 and ϕ_2 using images, we use a simple approach based on the principle of specular reflection. A vertical planner mirror is rotated first and an EPI is generated. Two highlights on the standing mirror appear at angles $\phi_1/2$ and $\phi_2/2$. They are extracted from the EPI at the horizontal traces.

Fig. 8 shows an EPI taken from a real object with concave shapes. It is interesting to notice that the traces due to interreflection are near the concave shape generated highlight traces. Those two kinds of traces will not intersect with each other. This can be simply explained as follows. If a highlight trace intersects with a trace of interreflection at a point in the EPI, the rays directly from light and reflected from another object surface should be collinear. This will not happen since the surface interreflecting the ray will occlude the ray from the light.

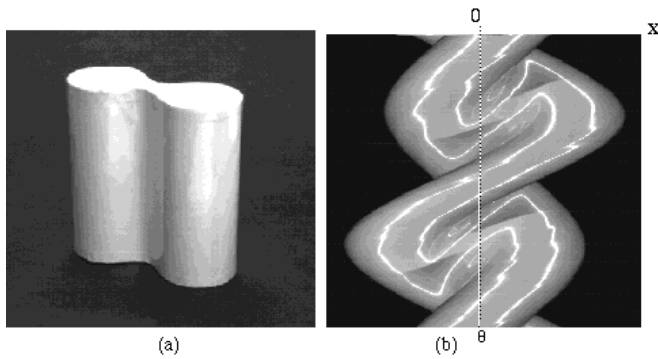


Fig. 8. A real object with concave shapes and one of its EPI under two light sources. (a) Object. (b) One of its EPI. Interreflection produced traces are curves with low intensity here.

5 SHAPE RECOVERY WITH SINGLE PLANE OF RAYS

If only one plane of rays is set, we can observe a highlight stripe on the object surface. Assuming the shape is not a plane, the highlight trace will not be horizontal in the EPI and we can take the derivative of (1) with respect to θ to obtain

$$x'(\theta) = X'_\theta \cos \theta + Z'_\theta \sin \theta - X \sin \theta + Z \cos \theta \quad (21)$$

The first two terms express a possible shift in the highlight on the surface and (X'_θ, Z'_θ) is the tangent of the shape in the rotation plane. From (1), (9), (21), two linear differential equations

$$\frac{\partial Z}{\partial \theta} \cos \alpha + Z \frac{\sin(\theta + \alpha)}{\cos \theta} = \frac{\partial x(\theta)}{\partial \theta} \sin(\theta + \alpha) + \tan \theta \sin(\theta + \alpha) x(\theta) \quad (22)$$

$$\frac{\partial X}{\partial \theta} \cos \alpha - X \frac{\cos(\theta + \alpha)}{\sin \theta} = \frac{\partial x(\theta)}{\partial \theta} \cos(\theta + \alpha) - \text{ctg} \theta \cos(\theta + \alpha) x(\theta) \quad (23)$$

can be deduced, when $\theta \neq \pi/2$, $3\pi/2$, and $\theta \neq 0$, π , respectively, to describe the highlight motion. These θ angles are singular points where the equations diverge. We use (22) within $[-\pi/4, \pi/4]$ and $[\pi - \pi/4, \pi + \pi/4]$, and use (23) within $[\pi/2 - \pi/4, \pi/2 + \pi/4]$ and $[3\pi/2 + \pi/4, 3\pi/2 + \pi/4]$ separately to avoid an inaccurate description near the singular points. As $Z(\theta)$ and $X(\theta)$ are obtained from (22) and (23) separately, their corresponding $X(\theta)$ and $Z(\theta)$

are computed using (1) accordingly. The solution can be summarized in the domain $[-\pi/4, \pi/4]$ and $[\pi - \pi/4, \pi + \pi/4]$ as

$$Z(\theta) = \left(\int_{\theta_i}^{\theta} \frac{\sin(\lambda + \alpha(\lambda))(X'_\lambda(\lambda) + x(\lambda) \tan \lambda)}{\cos \alpha(\lambda)} e^{\int_{\theta_i}^{\lambda} \frac{\lambda \sin(\tau + \alpha(\tau))}{\cos \alpha \cos \alpha(\tau)} d\tau} d\lambda + Z_{\theta_i} \right) e^{-\int_{\theta_i}^{\theta} \frac{\sin(\lambda + \alpha(\lambda))}{\cos \alpha \cos \alpha(\lambda)} d\lambda} \quad (24.1)$$

$$X(\theta) = (x(\theta) - Z(\theta) \sin \theta) / \cos \theta \quad (24.2)$$

and in the domain $[\pi/2 - \pi/4, \pi/2 + \pi/4]$ and $[3\pi/2 + \pi/4, 3\pi/2 + \pi/4]$ as

$$X(\theta) = \left(\int_{\theta_i}^{\theta} \frac{\cos(\lambda + \alpha(\lambda))(X'_\lambda(\lambda) + x(\lambda) \text{ctg} \lambda)}{\cos \alpha(\lambda)} e^{\int_{\theta_i}^{\lambda} \frac{\lambda \cos(\tau + \alpha(\tau))}{\sin \alpha \cos \alpha(\tau)} d\tau} d\lambda + X_{\theta_i} \right) e^{-\int_{\theta_i}^{\theta} \frac{\cos(\lambda + \alpha(\lambda))}{\sin \alpha \cos \alpha(\lambda)} d\lambda} \quad (25.1)$$

$$Z(\theta) = (x(\theta) - X(\theta) \cos \theta) / \sin \theta \quad (25.2)$$

In the solutions, $(X_{\theta_i}, Z_{\theta_i})$ is a known point on the surface establishing a boundary condition. The trace of the known point crosses with the highlight trace at angle θ_i . Starting from $(\theta_i, x(\theta_i))$, we compute integrals along the highlight traces. Although there are terms of $\partial x / \partial \theta$ in (24) and (25), they disappear in numeric calculation. To improve the accuracy of the solution, we take images at small rotation intervals, which makes the summation close to integrals in the solution.

If the plane of rays is along the camera axis, the angle α for all points are zero, and the solution becomes even simpler. In a rotation plane, at least one point is needed as a boundary condition for solving a complete shape. Increasing the number of known points will improve accuracy of the shape recovered from the integral. The boundary conditions are either from fixed points the highlight passes [8] or from one end of the trace whose position is obtained from the connected highlight trace, as well as contours if the surface is convex [7], [11]. A trace of a corner connects a highlight trace, while the trace of a texture point intersects a highlight trace without breaking it (Fig. 9). At those crossing points, 3D positions are computed accurately from traces of fixed points by the least-squared error method. We start the estimation of the smooth surface there by computing integrals along highlight traces, until a point with a horizontal tangent is reached. Then we modify the direction of the integral (from increasing θ to decreasing θ or vice versa) for further propagation of shapes.

6 EXPERIMENTS

Generally, tracking a highlight or specular feature in the original images is not easy because such features split and merge at the surfaces of an object and their sizes change according to shape curvature (see (14)). On a surface with a low absolute value of curvature, feature size becomes large so that its position is hard to be located accurately in the image, and the image velocity is high, according to (11). By using an EPI, however, such quick moving features can be accurately located from their traces by filtering the EPI vertically.

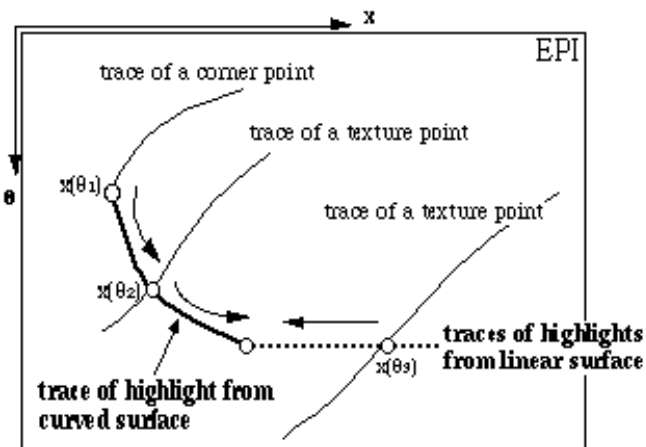


Fig. 9. Estimation of a smooth shape in the rotation plane starting from fixed points (texture edges or corners). An EPI is depicted, where a highlight trace crosses the traces of fixed points at $x(\theta_1)$, $x(\theta_2)$, and $x(\theta_3)$. From the intersecting points, the highlight is followed and the integral which yields 3D positions of surface points is computed.

For fixed points from pattern edges and corners, a step edge detector filters EPI horizontally and vertically to obtain their locations. For a shiny surface, the operator also picks up the edges of highlights. To detect highlights, a ridge-type operator is used horizontally and vertically to find locations with extreme intensities. If the intensity at a point is higher than a threshold and the point is bounded by two edges, we consider it a highlight. Edges near the output of the ridge operator are removed since they are boundaries of a highlight. Fixed points can be verified further by fitting a sinusoidal curve to a set of tracked points in the EPI and then checking the remaining error.

We have done experiments on both simulated objects and real objects. Fig. 10a displays a simulated EPI from a cylinder with two highlight traces, from which the shape on the rotational plane is correctly computed (Fig. 10b). For the real cylinder in Fig. 8a, we put it on a turntable and a camera with a long focal length was set about 2.5 m away from the object. Linear fluorescent lamps were set on two sides of the camera. A tracked EPI of the object is given in Fig. 11a and the estimated model is shown (Fig. 11b). We also tested a bottle (Fig. 12). The shapes were estimated using many rotational planes and the model was connected by graphics patches (Fig. 12b).

Under a single plane-of-rays illumination, Fig. 13 shows simulated EPIs from two cylinders; the light is from camera direction ($\phi = 0$) and the rotation axis is at the center of the cylinder. Since there is no horizontal tangent of the trace in the EPI, no plane or concave shape exists on the rotational plane. In each EPI, a black surface point draws a trace as a sinusoidal curve. The integral is computed around the shapes from the only fixed points, which is the hardest condition for the shape computation. The obtained shapes are in Fig. 13b, which verify that the solution is correct and the accumulated error of the integral is small. More fixed points on the surface will reduce the ranges of the integral and provide more starting points. Because the accuracy of fixed points is higher than that of the highlights computed from the integral, it will improve the accuracy of the recovered shapes. For real objects, a bottle was put on the rotation table (Fig. 14) and the light came from the same direction as the camera. For objects with concave shapes, Fig. 15 displays the recovered model of the object in Fig. 8 from a single highlight.

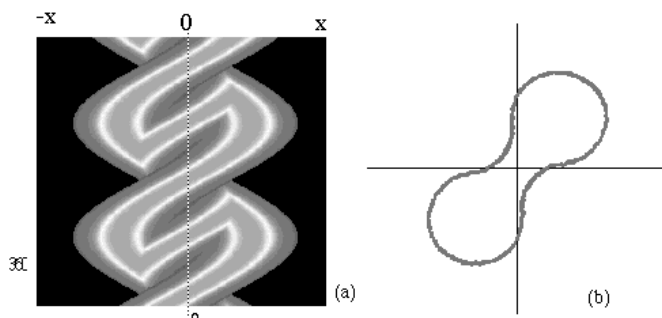
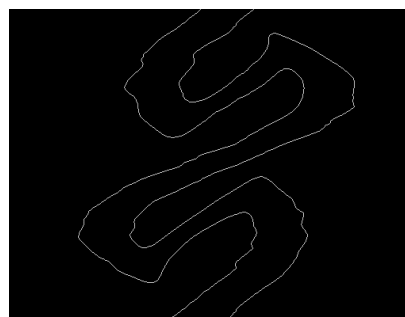
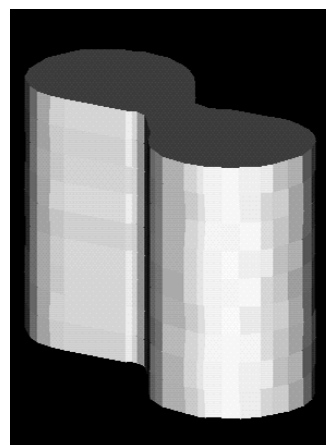


Fig. 10. A simulated EPI from a cylinder and the recovered shape under the illumination of two light sources. The result is very accurate.

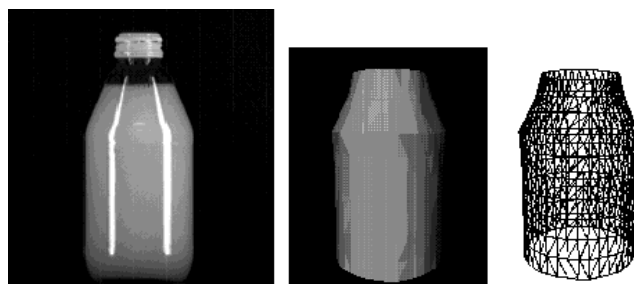


(a) Tracked highlight traces



(b) Connected shapes of each rotational plane (y interval is 10 pixels and θ interval is 10 degrees).

Fig. 11. Recovered model of the real object (given in Fig. 8) from two highlights.



(a) Object

(b) Recovered model displayed in shading and wire frame

Fig. 12. A bottle and its recovered model under two light sources.

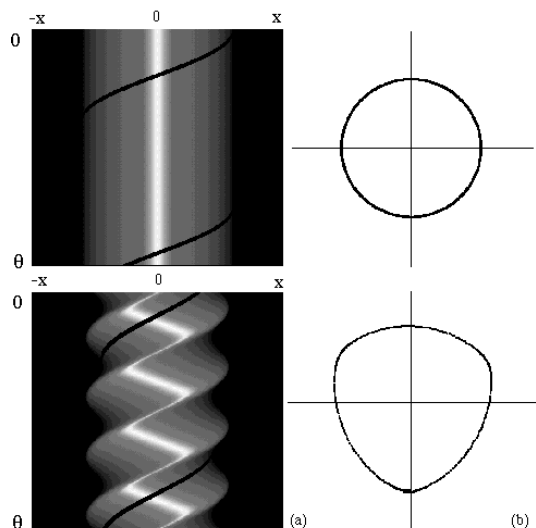


Fig. 13. Simulated EPIs from cylinders and their recovered shapes under a single light. (a) EPIs. (b) The recovered shapes.

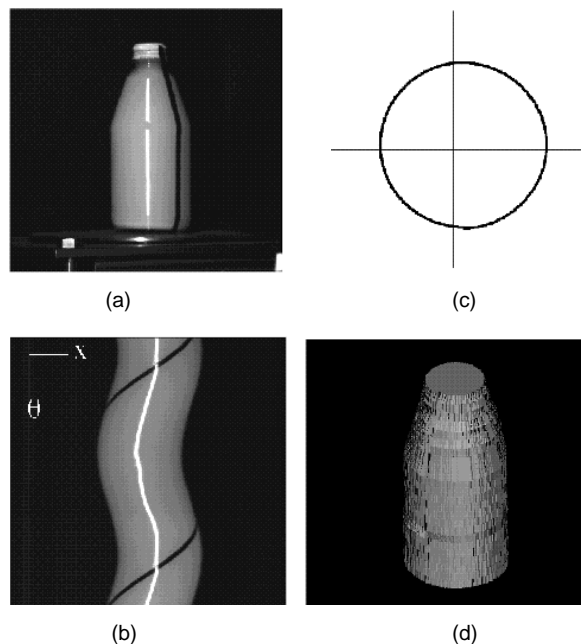


Fig. 14. Modeling a real bottle under one light source. (a) A bottle. (b) One EPI with the traces of a highlight and a fixed point. We can notice the bottle is not centered at the rotation axis. (c) One recovered cross section. (d) The whole model in graphics patches.

7 CONCLUSION

In this paper, we described new methods for the qualitative identification and quantitative recovery of 3D shapes with specular reflectance. We rotate an object and illuminate it by extended lights in one or multiple planes of rays. By detecting highlight motions in the rotation planes and computing directions of highlight stripes in the images, the object surface can be recovered at each point. Two simple methods proposed are direct computations of shapes using linear equations and first-order linear differential equations. Qualitative analysis of the highlight traces in the EPIs provides global shape information for model construction. We construct 3D surfaces and then models of real objects.

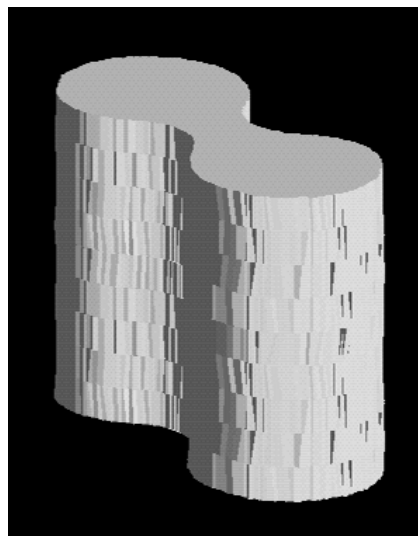


Fig. 15. Recovered model of the object given in Fig. 8 with a single highlight.

REFERENCES

- [1] K. Ikeuchi, "Determining Surface Orientations of Specular Surfaces by Using the Photometric Stereo Method," *IEEE Trans. Pattern Analysis and Machine Intelligence*, vol. 3, no. 6, pp. 661-669, 1981.
- [2] H. Baker and R. Bolles, "Generalizing Epipolar-Plane Image Analysis on the Spatiotemporal Surface," *CVPR-88*, pp. 2-9, 1988.
- [3] G. Klinker, S. Shafer, and T. Kanade, "The Measurement of High-Lights in Color Images," *IJCV*, vol. 2, no. 1, pp. 7-32, 1988.
- [4] A. Black and G. Brellstaff, "Geometry from Specularities," *Second ICCV*, pp. 394-403, 1988.
- [5] A. Zisserman, P. Giblin, and A. Blake, "The Information Available to a Moving Observer from Specularities," *Image and Visual Computing*, vol. 7, pp. 287-291, 1989.
- [6] C. Bellver-Cebreros and M. Rodriguez-Danta, "Caustics and the Legendre Transform," *Optics Comm.*, vol. 92, nos. 4-6, pp. 187-192, 1992.
- [7] J.Y. Zheng, "Acquiring 3D Models from Sequences of Contours," *IEEE Trans. Pattern Analysis and Machine Intelligence*, vol. 16, no. 2, pp. 163-178, Feb. 1994.
- [8] J.Y. Zheng, Y. Fukagawa, T. Ohtsuka, and N. Abe, "Acquiring 3D Models from Rotation and a Highlight," *12th ICPR*, vol. 1, pp. 331-336, 1994.
- [9] H. Schultz, "Retrieving Shape Information from Multiple Images of a Specular Surface," *IEEE Trans. Pattern Analysis and Machine Intelligence*, vol. 16, no. 2, pp. 195-201, 1994.
- [10] J.Y. Zheng, Y. Fukagawa, and N. Abe, "Shape and Model from Specular Motion," *Fifth ICCV*, pp. 92-97, 1995.
- [11] M. Oren and S.K. Nayar, "A Theory of Specular Surface Geometry," *Fifth ICCV*, pp. 740-747, 1995.
- [12] J. Clark, E. Trucco, and H. Cheung, "Improving Laser Triangulation Sensors Using Polarization," *Fifth ICCV*, pp. 981-986, 1995.